1

An Introduction to Chiral Nanomaterials: Origin, Construction, and Optical Application

Zhengtao Li, Lin Shi, and Zhiyong Tang

The National Center for Nanoscience & Technology, No. 11 Beiyitiao, Zhongguancun, Beijing 100190, China

1.1 Introduction

Chirality has aroused extensive interest in both science and technology since its first observation in the early nineteenth century [1–3]. Generally speaking, chirality is related to a structure without S_n symmetry elements, such as mirror plane (σ), and inversion (i) symmetry. For instance, an organic molecule with chiral carbon atom that is connected with four different functional groups is a typical chiral system (Figure 1.1). Understanding chirality at molecular level has led to enormous growth in multidisciplinary fields. In biology, it is believed to be one of the keys for understanding the life origin and evolution [4]. Two basic biomolecule building blocks, amino acid (L-form) and nucleotide (D-form) of homochirality, assemble into second- or higher-order structures, which could further evolve into different functional organisms. In medicine, many synthetic drugs of the specific chirality could be used to cure disease, whereas its isomer acts in the opposite way [5, 6]. Accordingly, chiral organic synthesis based on catalysis and postseparation has become one of the hottest research topics in chemistry [7–9]. Tremendous advances have been achieved in preparation of chiral drugs, and even the full synthesis of chiral biomacromolecules is available [10].

Extending the chirality from molecules to nanomaterials is bringing many new opportunities for the chiral study [11, 12]. Nanomaterials of the sizes ranging from 0.5 to 100 nm actually act as a bridge for the chiral study between molecules and bulk materials. The unique physical and chemical properties of nanomaterials could be easily tuned by altering their size, shape, or ingredient, providing a powerful platform for exploring the chiral properties [13–15]. For example, we can manipulate the chiral optical activity to any target wavelength just by controlling the size of nanomaterials, which is difficult and troublesome for organic molecules [16]. Furthermore, additional action modes such as multipole–multipole coupling [17, 18], which are normally ignored in small molecules and become increasingly important in nanoscale objects, are bringing new insights into conventional chiral optics mainly based on dipole–dipole interaction. Except for fundamental research, chiral nanomaterials offer potential novel applications [19]. As an example, grafting chiral biomolecules onto

Chiral Nanomaterials: Preparation, Properties and Applications, First Edition. Edited by Zhiyong Tang.

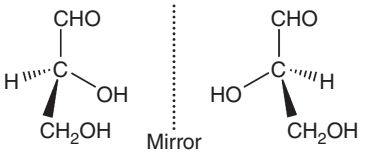

Figure 1.1 Scheme of chiral organic molecules.

the nanomaterial surfaces might generate multifunctional binding sites, which are more efficient to crosslink with surface receptors. Therefore, nanomaterials not only act as the simple carriers of chiral biomolecules but also play an active role in biomedical applications [20]. Our recent work has distinguished the obvious difference in the interaction efficiency between the living cells and the nanoparticles modified with biomolecules of the opposite chirality [21].

In the last five years, we witnessed many outstanding works about synthesis, property, and application of the chiral nanomaterials, and some excellent reviews related to this topic have been published [3, 11, 12, 22, 23]. It should be noted that most previous publications are focused on introduction of the chiral properties of the nanostructures obtained with the help of organic molecular assemblies [1, 24–26], and nevertheless there is absence of systematic summary on chiral noble metal structures, especially Au and Ag nanoparticles, though they have been proved to possess very specific optical activity. Here, we will summarize the-state-of-art progress of chiral noble metal nanoparticles in detail. First of all, the basic knowledge about the chiral optical spectra is briefly introduced. Next, the origin and construction of chiral metal nanoclusters are discussed. Subsequently, chiral nanoparticles or nanoparticle assemblies with characteristic optical activity are covered. Finally, the applications and perspectives of chiral noble metal nanostructures are presented. It should be noted that because the enantioselective catalysis by using chiral noble metal nanostructures has been extensively summarized in recent reviews [11, 12], herein the application of chiral noble metal nanostructures will be concentrated in the field of optics.

Among different properties, the optical activity is one of the most important features of chiral molecules, which is extensively characterized by circular dichroism (CD) spectrum [12]. The detection principle of CD spectra is as follows: When two circular polarized lights (CPLs) of same intensity and frequency but opposite direction are passed through a chiral sample, the difference in CPL absorption leads to production of the elliptically polarized light. The CD effect of a chiral molecule could be generally expressed by the following equation [27, 28]:

$$\mathrm{CD} \propto \mathrm{Im}\left[\mu_{12} \cdot m_{21}\right] \tag{1.1}$$

where μ_{12} and m_{21} are the electric and magnetic dipole moments of a molecule, respectively.

In addition to CD spectra, other methods including vibrational circular dichroism (VCD) and optical rotatory dispersion (ORD) are also broadly used for measuring the optical activity of chiral molecules. The main difference between CD and VCD is optical wavelength. CD spectra located at the UV–vis region could be used for analysis of the second- or higher-order structures of chiral molecules, whereas VCD located at the infrared region might be adopted to determine the

structure and absolute configuration of molecules. As for ORD and CD, ORD is based on the scattering difference when CPL lights are passed through a chiral medium, while CD is originated from the absorption difference. The ORD and CD spectra might be easily converted via the Kronig–Kramers equation. Notably, all the above spectra even could also be combined with other techniques such as high-performance liquid chromatography (HPLC) or synchrotron radiation system to meet more complicated needs for chiral molecules [29, 30].

1.2 Chiral Noble Metal Clusters

Clusters are a special class of nanomaterials, which contain few atoms of the characteristic sizes ranging from 0.5 to 2 nm. Different from the normal noble metal nanoparticles with the sizes of 2–100 nm, the extremely small metallic cores of the clusters are susceptible to the surrounding organic shells, resulting in chirality inside the clusters. Moreover, the quasi-continuous energy levels of noble metal clusters are opened with size shrinkage, generating the strong quantum confinement and exciton localization [31]. This is the reason why we use a separate chapter in this review to introduce the chiral noble metal clusters. The noble metal clusters are generally expressed as $M_x(L)_y$, where M and L stand for the metal element and organic ligand, respectively, and the subscripts x and y denote the corresponding number of metal atoms and ligands. The metals refer to Au and Ag, while the ligands could be various organic molecules such as phosphine [32] and thiols [33].

1.2.1 Origin of Chiral Noble Metal Clusters

Typically, three mechanisms have been proposed on the chirality origin of metal clusters: (i) chiral metal core; (ii) dissymmetric field model; and (iii) chiral footprint model. As for the chiral cores, Garzon *et al*. used Hausdorff chirality measure to calculate the intrinsic structure of noble metal clusters, revealing that the lowest energy isomers of bare Au_{28} and Au_{55} clusters were chiral. Furthermore, the chirality index was found to increase after modification of cluster surfaces with achiral thiol molecules [34]. The second mechanism suggests that the chirality of the achiral cores is induced when they are placed in a chiral environment, such as a chiral adsorption pattern. The particle-in-a box module is adopted to explain the mechanism [35]. This module demonstrates that the chiral charges of the ligands could induce chiral images inside metal clusters, giving rise to the chiral electronic state of metal cores, while the structure of the cores remains achiral. Chiral footprint model is an intermediate one between the former two theories; that is, the chiral ligand absorption could lead to the surface atoms relaxation, creating a chiral footprint on the surface of metal clusters [36]. Double anchoring points of the ligand molecules seem to facilitate the formation of the foot prints on the surface of metal clusters. It should be pointed out that to separate these mechanisms in real samples is very difficult, especially when the ligands are chiral molecules. The reason is the fact that the organic ligands not only act as the stabilizers but also distort the surface of metal clusters. For instance, by using

the time-dependent density functional theory (TD-DFT), Garzon *et al*. disclosed that the chirality of [Au_{25}(glutathione)$_{18}$] clusters simultaneously originated from the slight structural distortion of the metal cores and the dissymmetric field of the organic ligands [37].

Fast development on the experimental characterization offers direct evidences to understand the origin of the chiral noble metal clusters. The X-ray structure survey on Au_{102}(*p*-mercaptobenzoic acid)$_{44}$ clusters showed that they are chiral, having two enantiomers alternating in the crystal lattice [38]. In single clusters, 89 of 102 Au atoms had fivefold rotational symmetry, whereas the rest of 13 Au atoms on the equator had no obvious symmetry. The "staple" motif formed by one Au atom acted as a bridge between two sulfur groups of *p*-mercaptobenzoic acid ligands. The arrangement of the staple structure on the surface of the metal clusters finally induced formation of the intrinsic chiral structure of metal clusters. Subsequent studies by many groups further indicated that either short or long staples were formed in different noble metal clusters such as Au_{28}(*p*-tert-butylbenzenethiolate)$_{20}$ [39], $Au_{38}(SC_{12}H_{25})_{24}$ [40, 41], and $Au_{144}(SC_{12}H_{25})_{60}$ [42]. The arrangement of these staples on the surface of the clusters highlighted the chirality origin inside these noble metal clusters.

1.2.2 Construction of Chiral Noble Metal Clusters with Optical Activity

An early synthesis of colloidal chiral metal clusters was performed by Whetten group [43, 44], and a series of glutathione-stabilized Au clusters were successfully obtained via gel electrophoresis separation. Interestingly, Au clusters with core masses ranging from about 4.3 to 8.2 kDa showed strong chiroptical activity switching from the near-infrared and visible to near-ultraviolet region with increase in size, demonstrating a gradual decrease in the band gap of Au clusters caused by strong quantum confinement effects. Different mechanisms, such as inherently chiral cores and chiral absorption pattern, were proposed to illustrate the formation of optical activity. However, due to the lack of precise knowledge of structure and sophisticated theoretical calculations, it is hard to determine the source of the chiroptical activity of Au clusters. In order to better understand their optical properties, metal cluster enantiomers have been synthesized. Yao *et al*. synthesized three chiral Au clusters with average sizes of 0.57, 1.18, and 1.75 nm, respectively, by using the enantiomer pair of penicillamine as stabilizers (Figure 1.2a and b) [45, 46]. The CD spectra of Au clusters, respectively, capped by L- and D-penicillamine displayed a mirror-image relationship with each other, while no obvious CD signal was detected when using rac-penicillamine as capping agents. This finding implies that chirality of Au clusters is closely related to the stereochemistry of the surface modifiers. Meanwhile, Yao *et al*. studied the stability of chiral Au clusters by changing the solution temperature. As shown in Figure 1.2c, the CD response decreased with increasing temperature and showed a stable thermal reversibility between different temperatures. The temperature-dependent CD change was attributed to the conformational equilibrium of L/D-penicillamine on the cluster surfaces at different temperatures. In addition to the Au clusters, chiral Ag clusters have been obtained using the similar strategy [47]. Meanwhile, chiral noble metal clusters could be obtained by

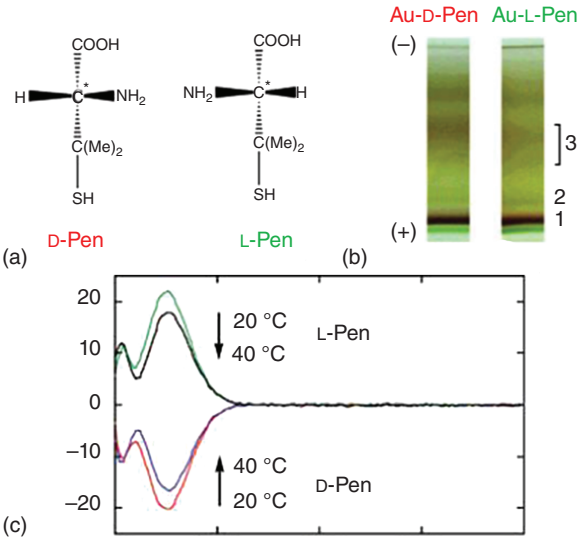

Figure 1.2 (a) Structure of chiral L/D-penicillamine, (b) electrophoresis separation of Au clusters, (c) temperature-dependent CD response. (Yao *et al*. 2005 [45] and Yao *et al*. 2007 [46]. Reproduced with permission of American Chemical Society.)

symmetry breakage of achiral clusters by postligand reaction or ligand exchange [48]. For instance, Bürgi *et al*. prepared the chiral Au nanoclusters through ligand exchange of Au_{38}(2-phenylethanethiol)$_{24}$ and Au_{40}(2-phenylethanethiol)$_{24}$ clusters with chiral monodentate or multidentate thiophenol [49, 50].

Besides the chiral ligands, the intrinsically chiral cores might give rise to the optical activity of the noble metal clusters [51]. The chiral $Au_{38}(SC_2H_4Ph)_{24}$ clusters induced by the surface staples were obtained by Bürgi *et al*. via chiral HPLC. Impressively, the mirror CD responses were observed for the Au cluster enantiomers. Since the SC_2H_4Ph ligand was achiral, the optical activity could only originate from the intrinsically chiral core. Moreover, the authors found that the enantiomers could reverse to each other through surface rearrangement involving the staple place exchange under mild temperatures (40–80 °C) without significant decomposition and complete Au—S bond breaking. The similar phenomenon has been discerned in other chiral noble metal clusters including Au_{28} clusters [52] and Au_{40} clusters [53].

1.3 Chiral Plasmonic Nanostructures

Chiral noble metal nanoparticles with a size larger than 2 nm are fundamentally different from their clusters. First of all, the intrinsically chiral cores are impossibly achieved with noble metal nanoparticles, because the large-sized cores usually are achiral crystalline structures. Moreover, noble metal nanoparticles of the sizes over 2 nm possess the continuous energy levels and abundant free electrons, leading to the strong interaction with external electromagnetic field. As a result, the unique local surface plasmon resonance (SPR) feature, rather than the excitons in metal clusters, is recognized for noble metal nanoparticles. Therefore, in order to differentiate from the noble metal clusters, we intentionally name the noble metal nanoparticles larger than 2 nm as the plasmonic nanostructures in this

chapter. Notably, the SPR characteristics of the plasmonic nanostructures are closely related to their shape, composition, and size [15, 54–56], and even the arrangement inside nanoparticle assemblies [57, 58]. Combining chirality with plasmonic nanostructures will bring new insights into nanoscale chirality as well as chiral optics.

1.3.1 Origin of Chiral Plasmonic Nanostructures

Because the chiral plasmonic structures obtained by top-down physical strategy have been discussed in detail in a recent review [59], in this chapter we focus on the chemically synthesized chiral plasmonic nanostructures. Different models have been proposed to elucidate the origin of chiral plasmonic nanostructure. Firstly, single nanoparticle with surface chiral morphology was proposed recently. According to the definition of chirality, a structure without symmetry should be chiral, which is rather easily realized on the surface of plasmonic nanoparticles. As an example, by using chiral molecules as a template to *in situ* synthesize the nanoparticles, the molecular chirality could be imparted onto the nanoparticle surfaces. The twister or antitwister on the surface of plasmonic nanoparticles is believed to produce the strong CD signals, whereas the weak CD signals are expected to be achieved with spherical nanoparticles with slightly tetrahedral distortion [60] (Figure 1.3). Furthermore, lithography technique is also used to prepare the chiral structure, for instance, Kotov *et al*. synthesized three-dimensional (3D) chiral plasmonic nanostructures with strong optical activity in the visible light region by controlling the deposition angle of Au atoms on achiral ZnO nanopillars [61].

Another mechanism is based on coupling between achiral nanoparticles and chiral environment. The coupling between the optical activity of chiral molecules and the SPR absorption of the plasmonic nanostructures could not only enhance the molecules' chiral signal but also induce a new plasmonic CD signal in the CD spectrum (Figure 1.4). As the characteristic CD responses come from the chiral molecules and plasmonic nanoparticles, it can be written in two parts [62, 63]:

$$\mathrm{CD}_{\mathrm{molecule-NP}} = \mathrm{CD}_{\mathrm{molecule}} + \mathrm{CD}_{\mathrm{NP}} \tag{1.2}$$

Considering the difference in absorption of molecules and nanoparticles on the two incident electromagnetic waves of the polarized light, the equation would be

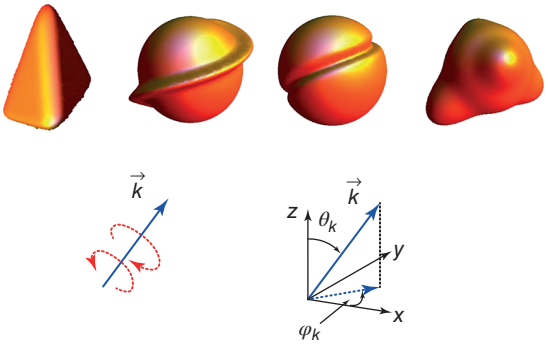

Figure 1.3 Nanoparticles with chiral morphology. (Fan and Govorov 2012 [60]. Reproduced with permission of American Chemical Society.)

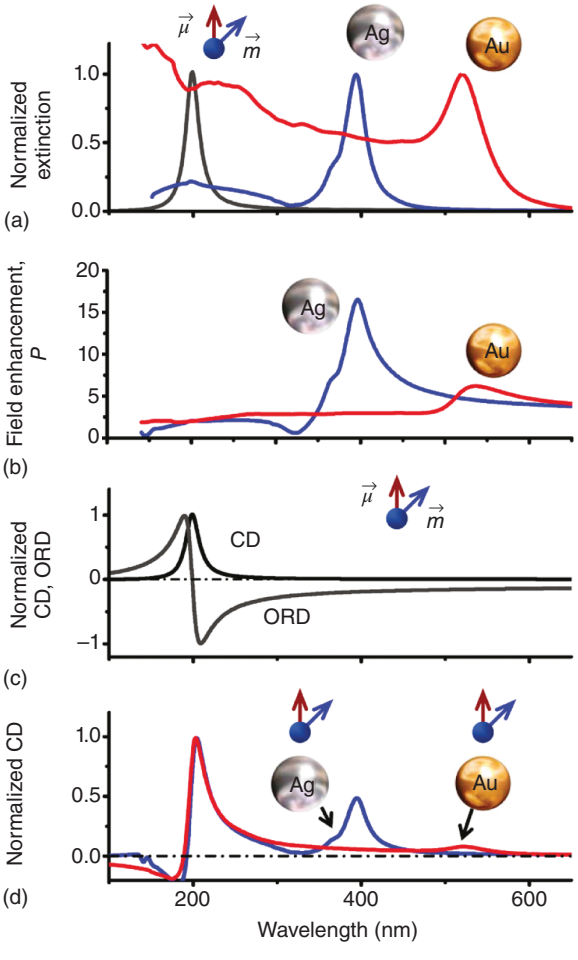

Figure 1.4 Coupling model of chiral molecules and plasmonic nanoparticles. (a) Absorption spectrum of metal nanoparticles, (b) field enhancement effect, (c) chiral signal of chiral molecules, (d) coupling between chiral molecules and plasmonic nanoparticles. (Govorov 2011 [62]. Reproduced with permission of American Chemical Society.)

expressed as follows:

$$\begin{aligned} \mathrm{CD}_{\mathrm{molecule}} &= \left\langle Q_{\mathrm{molecule},+} - Q_{\mathrm{molecule},-} \right\rangle_{\Omega} \\ &= {E_0}^2 \frac{8c}{3} k \cdot \frac{\Gamma_{12}}{\left| \left(\hbar\omega - \hbar\omega_0 + i\Gamma_{12} \right) - G(\omega) \right|^2} \mathrm{Im}\left[\left(\hat{P} \cdot \vec{\mu}_{12} \right) \cdot \vec{m}_{21} \right] \end{aligned} \quad (1.3)$$

$$\mathrm{CD}_{\mathrm{NP}} = \left\langle Q_{\mathrm{NP},+} - Q_{\mathrm{NP},-} \right\rangle_{\Omega}, Q_{\mathrm{NP},\pm} = \mathrm{Im}\left(\varepsilon_{\mathrm{NP}} \right) \frac{\omega}{2\pi} \int_{V_{\mathrm{NP}}} \mathrm{d}V \cdot \vec{E}^{\mathrm{in}}_{\omega,\pm} \vec{E}^{\mathrm{in}*}_{\omega,\pm} \quad (1.4)$$

The enhancement of chiral molecule's CD signal is caused by the plasmon-induced change in the electromagnetic field near the chiral molecule (Equation (1.2) and Figure 1.4b). Meanwhile, as most molecules have chiral signal in the UV region, new plasmonic CD response, which is located at the characteristic wavelength of SPR absorption, is resulted from the chiral-molecule-induced chiral current inside the plasmonic nanoparticles (Equation (1.3), Figures 1.3 and 1.4a). The intensity of both CD signal of chiral

molecules and plasmonic CD response of nanoparticles are highly dependent on the coupling strength between chiral molecules and plasmonic nanoparticles, for example, the size of nanoparticles, the orientation of chiral molecules on the nanoparticle surfaces and the center-to-center distance between molecules and nanoparticles [64]. In addition, the effective coupling between chiral molecules and plasmonic nanoparticles may be tuned by altering the characteristic optical absorption of molecules or nanoparticles. As an example, Itai *et al*. found that, after binding the chiral molecules (L-glutathione-bimane) onto the surface of Ag nanoparticles, the CD intensity was enhanced by about 100 times than that of molecules, due to very close optical absorption peaks of L-glutathione-bimane molecules at 390 nm and Ag nanoparticles at 400 nm [65].

Except for the above-mentioned near-field dipole–dipole coupling that is normally happened within few nanometers, far-field radiative coupling between chiral molecules and plasmonic nanoparticles is also reported [66]. The Au cross array with different nominal thicknesses of 55, 100, and 130 nm was fabricated by electron beam lithography technique. After depositing chiral molecules, CD intensity was enhanced by increasing the nominal thickness of the Au cross array. As the Au cross array could not yield strong dipole–dipole interaction with chiral molecules and the opposite decay tendency against near-field dipole–dipole coupling was observed, the enhancement of chiral signal was attributed to the far-field coupling between chiral molecules and the plasmonic nanostructures. This new coupling mode extends the flexibility of construction of chiral plasmonic nanostructures.

The above two mechanisms have been broadly used for explanation of the origin of single chiral plasmonic nanoparticles. An alternative mechanism to elucidate origin of chiral plasmonic nanoparticle assembly instead of individual plasmonic particles involves the Coulomb interaction among the nanoparticle building blocks in the assembly. The CD spectrum of plasmonic nanoparticle assembly could be calculated based on the dipole–dipole electromagnetic interaction:

$$\varepsilon_{\mathrm{CD}} = \left\langle \varepsilon_{+} - \varepsilon_{-} \right\rangle_{\Omega}$$
$$\varepsilon_{\pm} = \left(\frac{N_{\mathrm{A}}}{0.23} \right) 10^{4} \varepsilon_{0} \frac{8\pi}{2 \cdot E_{0}^{2} \cdot c_{0} \sqrt{\varepsilon_{0}}} \omega \mathrm{Im} \left[\sum_{i} \frac{\vec{d}_{i,\pm}^{*} \cdot \vec{d}_{i,\pm}}{\alpha_{i}^{*}(\omega)} \right] \tag{1.5}$$

Many parameters including nanoparticle geometry, interparticle distance, and composite of the assembly have a big effect on the final CD signal. Generally speaking, chiral assembly with asymmetric frames results in strong CD signals [67]. As an example, the helix assembly structure has the largest optical anisotropy factor, whereas the equilateral tetrahedral nanoparticle assembly shows the smallest CD signals (Figure 1.5). Meanwhile, increasing the size of nanoparticles in the assembly or reducing the distance between them improves optical activity. A very important advantage of the chiral plasmonic assembly is that its CD responses are very stable against varying defects such as missed nanoparticles, inconsistent pitch length, and positional disorder of building blocks in space [68]. It should be noted that except for the well-known

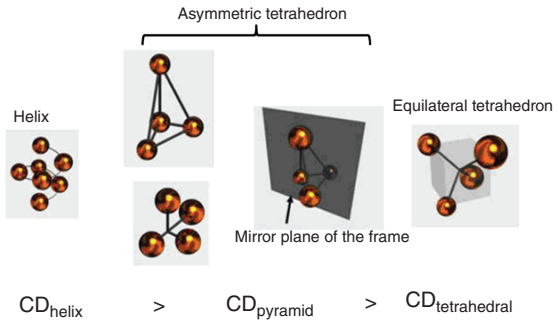

Figure 1.5 Different types of chiral assembly. (Fan and Govorov 2010 [67]. Reproduced with permission of American Chemical Society.)

dipole–dipole interaction between nanoparticles, multipole–multipole interaction is also crucial for plasmonic CD of the assembly. For instance, the dipole–dipole interaction between nanoparticles in the equilateral tetrahedral assembly of four nanoparticles has no any contribution to the CD signal, so the weak but clear CD signal of the assembly should solely come from the multipole–multipole interactions. The unique multipole–multipole interaction between plasmonic nanoparticles is significant for extending the conventional CD theory that is mainly based on the dipole–dipole interaction between molecules.

The chiral assembly models were further developed by Liz-Marzan *et al*. by adopting the anisotropic Au nanorods as the building block [69]. Typically, the minimum number of spherical Au nanoparticles to construct a chiral pyramid is four, whereas only two Au nanorods are needed to produce the chiral arrangement due to the presence of the dihedral angle between them (Figure 1.6a). Furthermore, the plasmonic CD signal of the bisignated line shape is observed for the cross Au nanorod couple (Figure 1.6b), which is originated from the antisymmetric and symmetric hybrid modes. The retardation effect and the coupling between longitudinal and transverse modes lead to the asymmetry in the CD signal. Recently, Xu *et al*. found that the heterodimers of Au nanoparticles of different sizes could produce the distinct CD signal, and, moreover, the mirror image of the chiral signals was achieved with different induced molecules such as DNA or sodium chloride. Considering that the shape of Au nanoparticles was not perfect spherical, small dihedral angel between the heterodimers of Au nanoparticles was believed to be the asymmetric factor in the heterodimers [70].

It should be stressed that although several mechanisms have been proposed, it is not easy to assign the origin of chiral plasmonic structure to one type of mechanism in the real cases. Analogously to the origin of chiral metal clusters, these mechanisms are at work simultaneously, while a small change in the parameters may lead to alternation of the dominant mechanisms. For example, Markovich *et al*. synthesized chiral silver nanoparticles and analyzed their optical activity by the temperature-dependent CD spectroscopy [71]. The Ag nanoparticles of small sizes showed a temperature-dependent CD intensity at 400 nm. The reduced plasmonic CD signals of small Ag nanoparticles with increasing temperature might be attributed to the thermally agitated disordered adsorption of the chiral ligands on the nanoparticle surfaces. Therefore, as for small Ag nanoparticles,

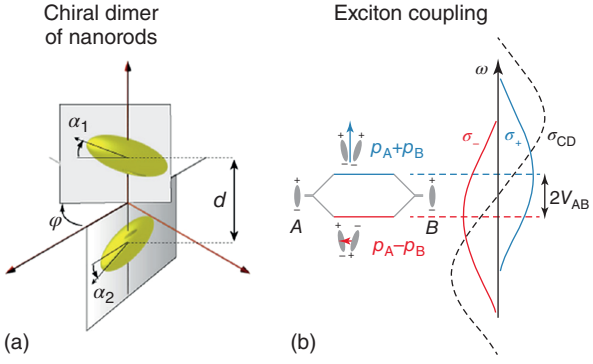

Figure 1.6 Chiral dimmer of ellipsoid nanoparticles (a) and LSPR hybridization (b) with symmetric mode $\omega+$ and an antisymmetric mode $\omega-$. (Auguie *et al.* 2011 [69]. Reproduced with permission of American Chemical Society.)

the origin of plasmonic CD response was mainly caused by coupling between SPR of Ag nanoparticles and the chiral signal of organic ligands. On the contrary, with respect to Ag nanoparticles of large sizes, the CD signal with much stronger intensity displayed the temperature-independent property. Both the theoretical calculation and the experimental characterization demonstrated that the large Ag nanoparticles were covered by a monolayer of organic ligands of the chiral stacking. Hence, the mechanism of the large Ag nanoparticles of a helical groove was proposed to be dominant for the CD response.

1.3.2 Construction of Chiral Plasmonic Nanoparticles with Optical Activity

The direct mixture of metal precursors with chiral organic ligands in the solution is the most convenient way to prepare the chiral plasmonic nanoparticles. Because the chiral molecules are normally used as the capping ligands, the chirality is thought to impart onto the surface of synthesized nanoparticles, giving rise to the chiral surface of plasmonic nanoparticles. Kotlyar *et al.* utilized a long-chain DNA as a template to synthesize the chiral Ag nanoparticles [72]. Owing to many nitrogen groups in DNA bases and the electrostatic attraction between Ag^+ and DNA, Ag^+–DNA complexes were formed when mixed. After adding the reducing agent of $NaBH_4$ into the mixture solution, the bisignated CD signal centered at the characteristic SPR wavelength of 425 nm was discerned for as-synthesized Ag nanoparticles (Figure 1.7). In order to understand the origin of CD signal, the authors further mixed the prepared Ag nanoparticles with DNA. They found that the assembly pattern on the DNA scaffolds is same for the *in situ* synthesized Ag nanoparticles and the mixture of the prepared Ag nanoparticles. However, there was no CD signal to be observed from the mixture of the prepared Ag nanoparticles with DNA, disclosing that the chiral metal nanoparticles should be formed during the *in situ* synthesis process. The high-resolution transmission electron microscopy (HR-TEM) images also revealed that there were many defects on the surface of Ag nanoparticles growing on the DNA scaffold. The CD signal of such Ag nanoparticles could not be eliminated after separating the Ag nanoparticles from the long-chain DNA by cutting the DNA with deoxyribonuclease, further proving that the induction of chirality originated from the metal cores [73]. The formation of chiral silver nanoparticles was also proposed when

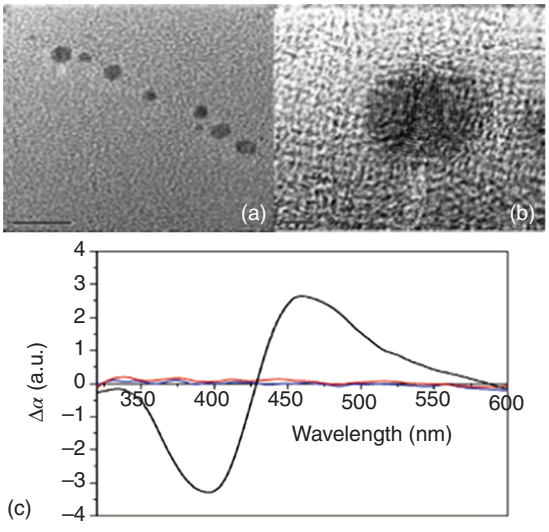

Figure 1.7 (a) Low and (b) high magnification of Ag nanoparticles and (c) corresponding CD spectrum. (Shemer *et al*. 2006 [72]. Reproduced with permission of American Chemical Society.)

the silver nanoparticles was *in situ* reduced from other chiral molecules system [71].

When the size of nanoparticles increases, it is not easy for nanoparticles to maintain their chiral metal cores due to the low ratio of surface atoms and the ordered and achiral crystal lattice. Thus, many synthetic strategies of large chiral plasmonic nanoparticles involve conjugation of large plasmonic nanoparticles with chiral molecules, especially for biomolecules of strong optical activity such as amino acids, peptides, and DNA. Govorov *et al*. synthesized chiral plasmonic nanoparticles by grafting two peptides with different secondary structure (random coil and β-helix) onto the surface of 10-nm Au nanoparticles [74], resulting in the appearance of plasmonic CD response. Based on the multiple interactions between the functional groups of the coated peptides, nanoparticle assembly might be formed. The Au nanoparticle assembly showed the enhancement and redshift of the plasmonic CD peaks, demonstrating the stimulation-responsive capability of the chiral plasmonic nanoparticles.

The improvement of SPR intensity of the plasmonic nanoparticles as well as the coupling between chiral molecules and the nanoparticles are beneficial for obtaining high optical activity. For example, Markovich *et al*. reported that the cholate-coated Ag nanoparticle assembly was destructured into individual Ag nanoparticles by increasing pH of the solution, meanwhile the CD signal disappeared. Therefore, the authors concluded that the hot spots inside the Ag nanoparticle assembly contributed to generation of plasmonic CD response [75]. Compared with spherical nanoparticles, the anisotropic plasmonic particles are thought to possess a much stronger electromagnetic field, which is crucial for the enhancement of optical activity. Tang *et al*. constructed a one-dimensional (1D) assembly of Au nanorods and cysteine, displaying strong optical activity [76]. The coupling between CD signal of cysteine isomers at 200–250 nm and the SPR absorption of Au nanorods resulted in the mirror image of plasmonic CD responses in the visible region. The chiral signals were easily tuned by changing

the aspect ratio of Au nanorods. Meanwhile, the dramatic enhancement of the optical activity was also distinguished in the assembly compared with the individual cysteine-capped Au nanorods. As introduced in Section 1.3.1, another efficient method to increase the CD intensity is to enhance coupling between chiral molecules and the plasmonic nanoparticles. Unfortunately, the CD signal of chiral molecules is normally located at the UV region and hard to be tuned, while the SPL absorption wavelength of noble metal nanoparticles is in the range of the visible region, giving rise to difficulty in enhancement of coupling between chiral molecules and plasmonic nanoparticles. Alternatively, we adopted the chiral quantum dots as the CD signal source to coupling with metal nanoparticles. The chiral quantum dots with the size-dependent CD signals, which were originated from quantum confinement effect, were synthesized by using chiral cysteine as stabilizer. After assembling the chiral quantum dots with Au nanorods, the plasmonic CD signals of Au nanorods were observed. Compared with the cysteine-induced CD signal, the CD intensity of quantum dot and Au nanorod assembly was much stronger, highlighting that a quantum dot "bridge" between the chiral organic molecules and the noble metal nanoparticles was beneficial for improving its optical activity [77].

1.3.3 Construction of Chiral Plasmonic Assembly with Optical Activity

Assembly of noble metal nanoparticles into chiral nanostructures has been confirmed as a plausible way to generate high optical activity. It should be pointed out though some plasmonic nanoparticle assemblies are introduced in Section 1.3.2, all these assemblies do not possess the 3D chiral configurations. A big advantage of chiral nanoparticle assembly, which is different from the small-scale molecule assembly, is that it is big enough to be directly observed by electron microscopes such as high-angle annular dark-field scanning transmission electron microscopy (HAADF-STEM). As a result, the chiral plasmonic assembly provides a unique platform to investigate the relationship between the chiral structure and optical activity [78]. Over the past few years, different approaches including soft template, DNA molecules, and inorganic channels have been used as the platforms to arrange noble metal nanoparticles in the chiral way.

1.3.3.1 Soft-Template-Induced Chiral Plasmonic Assembly

Many macromolecules such as small molecular assemblies, artificial polymers, and natural peptides are of 3D chiral structures, which can be used as templates to obtain the chiral plasmonic structures [79]. Liz-Marzan *et al*. constructed the chiral plasmonic assembly through absorption of Au nanorods onto the surface of anthraquinone-based oxalamide fibers with chiral morphology [80]. It was found that Au nanorods preferred should be organized along the longitudinal direction of chiral fibers, leading to a strong plasmonic CD response. The control experiment indicated that when the spherical Au nanoparticles with the diameter of 15 nm were adsorbed on the chiral fibers, there was no plasmonic CD signal to be observed. So it was concluded that the 3D chiral arrangement of Au nanorods was responsible for the strong plasmonic CD signal. Except the small molecule assemblies, chiral polymer has been also adopted as scaffolds to fabricate the chiral plasmonic structures. Prasad *et al*. used the chiral

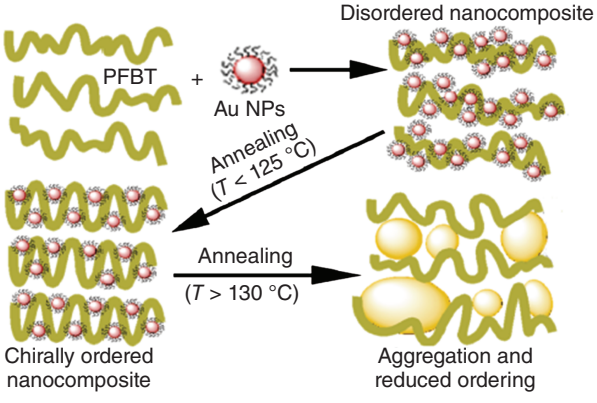

Figure 1.8 Scheme of chiral plasmonic assembly based on the polymer scaffold with extraordinary optical activity [81]. (Oh *et al*. 2010 [81]. Reproduced with permission of American Chemical Society.)

poly-(fluorene-*alt*-benzothiadiazole) (PFBT) as the scaffold for assembly of gold nanoparticles [81]. After modified with the PBFT fibers with 10-nm Au nanoparticles, a plasmonic CD peak was found. Interestingly, after annealing the film at 125 °C, the maximum CD intensity was obtained, which was more than 700 times than that of the origin nonannealing Au–PBFT complex. The chiral PFBT underwent an irreversible phase transition to the liquid crystalline state via thermal annealing, resulting in a dramatic enhancement of plasmonic CD response. With further increase in temperature to 150 °C, the transition of PFBT polymers to a less helical ordering occurred, leading to a decrease in the plasmonic CD signal (Figure 1.8). Interestingly enough, the assembly of ZnO nanoparticles and PBFT shows no CD response even after thermal annealing, demonstrating that the electronic coupling between the noble metal nanoparticles and PFBT was important for production of CD signal.

Since natural peptides could be synthesized in a large scale and exhibit chemical diversity in proteins, they have been often used as the building blocks for construction of various nanostructures including nanotubes, nanospheres, and nanofibrils [78, 82, 83]. These peptide nanostructures with varying secondary structures such as α-helix, random coil, and β-sheet could be further used as a scaffold for nanoparticle assembly. Rosi *et al*. combined the peptide self-assembly and nucleation of discrete nanoparticles together to synthesize the double-helical structure of Au nanoparticles (Figure 1.9) [84]. Left-handed twist assembly was obtained by supramolecule assembly of amphiphilic peptide C_{12}-AYSSGAPPMPPF (C_{12}-PEP_{au}). Owing to the strong interaction between the tyrosine residue of the peptide and the Au precursors, Au nanoparticles were *in situ* grown on the twist assembly of the peptide. The CD signals of such peptide-based chiral assemblies might be manipulated by changing the Au nanoparticle sizes and the interparticle distances. Moreover, *in situ* coating of the Ag shell on the chiral Au nanoparticle assembly led to an enhancement in the plasmonic CD response. Using the similar strategy, the plasmonic CD signal of the Au nanoparticle bunches on the protein tubes was also achieved. The

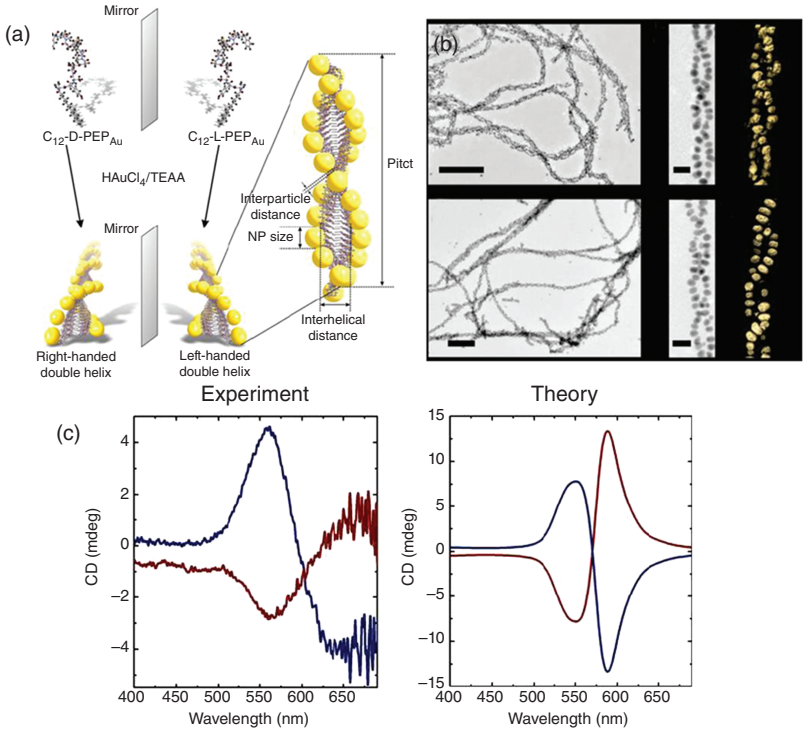

Figure 1.9 (a) Scheme, (b) transmission electron microscopy, and (c) CD spectrum of chiral assembly of Au nanoparticles and amphiphilic peptides. (Song *et al*. 2013 [84]. Reproduced with permission of American Chemical Society.)

assembly of Au nanoparticles was conducted by *in situ* reduction of $HAuCl_4$ on Au nanoparticle seeds protected by ethylene glycol thiol, which were preadsorbed onto the chiral diphenylalanine peptide nanotubes. Since there was no plasmonic CD signal to be discerned when the Au nanoparticles with the similar diameters of 4.5 nm were directly grafted onto the peptide nanotubes, it could be concluded that the preadsorbed Au nanoparticles act as the seeds for the subsequent growth of Au nanoparticle bunches and the chiral environment of the peptide nanotubes guaranteed the chiral arrangement of Au nanoparticle bunches [85].

1.3.3.2 DNA-Induced Chiral Plasmonic Assembly

DNA also belongs to one type of soft templates. However, different from usual soft templates, DNA possesses unique flexibility, designability, and programmability. As development of DNA nanotechnology especially DNA origami technology, many novel nanostructures have been fulfilled by design DNA sequences [86–89]. These nanostructures could act as a platform for the construction of nanoparticle assemblies with high precision and external response. Because many recent works are involved in DNA-based chiral plasmonic assembly, we intentionally employed a separate chapter to introduce it.

Alivisatos *et al*. adopted four single-stranded DNA (ssDNA) as the building blocks to construct the pyramidal DNA nanostructures, which could act as the template for chiral nanoparticle assembly [90]. Four Au nanoparticles were incorporated into the apexes of the pyramidal structures by modifying them with one of these four ssDNA. Inspired from the chiral carbon atoms in organic chemistry, four Au nanoparticles with different sizes were placed on the top point of pyramidal structures, resulting in generation of chiral Au nanoparticle assembly. The handiness of this structure was easily reversed just by changing the relative position of two Au nanoparticles in the pyramid structures. Although the authors did not characterize the optical activity of the chiral pyramid structures, this paper ignited the chiral assembly of the Au nanoparticles by using DNA molecules. After this work, many chiral structures induced by the DNA templates have been reported. Kotov *et al*. detected the plasmonic CD signals of Au nanoparticle assembly by carrying out the polymerase chain reaction (PCR) on the surface of Au nanoparticles [91]. By adjusting the density of the primers on the surface of Au nanoparticles and the PCR cycle numbers, different Au NP assemblies such as dimers, trimers, and tetramers were obtained. When the PCR cycle number was between 1 and 10, strong plasmonic CD signal could be observed. As the shape and size of Au nanoparticles were likely to be different from each other, some structures of Au nanoparticle assemblies were chiral, leading to production of plasmonic CD response. While the cycle number was passed 10, the Au nanoparticle assembly was found to contain spherical or cylindrical structures, leading to disappearance of optical activity. One of the drawbacks of the prepared chiral Au nanoparticle assembly is that the products were a mixture of many types of chiral structures and some nonchiral structures, so it is hard to attribute the optical activity to one type of special structure. In order to solve the problem, the same group synthesized the enantiomers of different chiral pyramids with a yield of about 80% based on different types of nanoparticles, for example, quantum dots, Ag nanoparticles, and Au nanoparticles (Figure 1.10a) [92]. The isomers with exact mirror CD images might be obtained by changing the related position of nanoparticles. The experimental results confirmed that when the pyramids were composed of four Au nanoparticles of the same size, the frame was symmetric and no obvious plasmonic CD signal was detected. As comparison, the symmetry was broken by changing the type or the size of nanoparticles. The strongest CD signal (1.9×10^{-2} at 520 nm and 1.7×10^{-2} at 422 nm) was obtained by using four different types of nanoparticles (Ag nanoparticles, quantum dots and Au nanoparticles of two different sizes) as the building blocks. It is worth mentioning that both plasmonic CD signals that were assigned to Au and Ag nanoparticles, respectively, were identified in the CD spectrum (right-hand side in Figure 1.10a).

Since Rothemund first used a long, ssDNA and several short, ssDNA (normally referred to as staple DNA) synthesized different two-dimensional (2D) nanostructures such as triangles, rectangles, or even smiley face, DNA nanostructures ranging from 1D to 3D have been widely constructed based on this technology [94–97]. This technology, often referred to as "DNA origami," provides a powerful ability for the construction of nanoparticle assemblies, in which accurate spatial arrangement of nanoparticles offers a convenient platform to manipulate

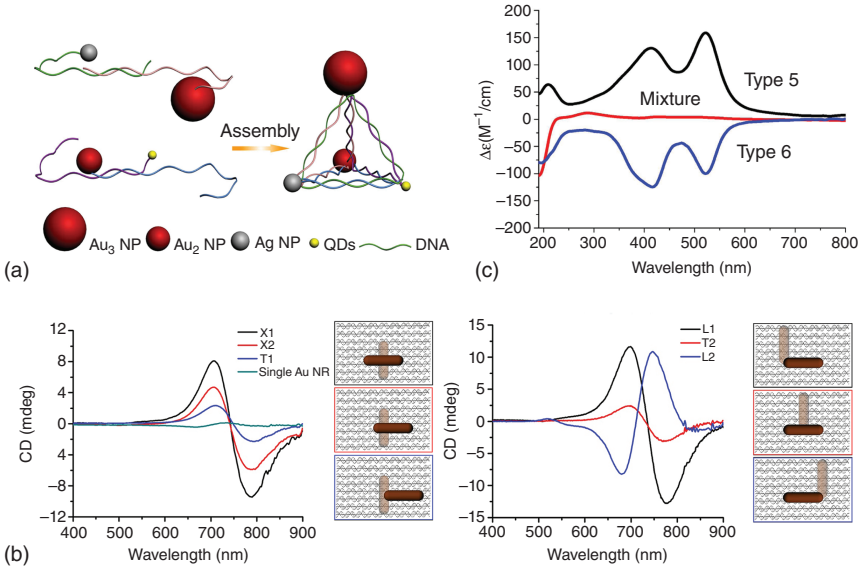

Figure 1.10 DNA-induced chiral assembly of plasmonic nanoparticles. (a) Pyramid of four different types of nanoparticles (Au nanoparticles of two sizes, Ag nanoparticles and quantum dots). (Yan *et al*. 2012 [92]. Reproduced with permission of American Chemical Society). (b) Au nanorod dimmers on planar DNA origami. (Lan *et al*. 2013 [93]. Reproduced with permission of American Chemical Society.)

their optical activity. Kuzyk *et al*. employed DNA origami 24-helix bundles to arrange nine Au nanoparticles in a helical arrangement with a high yield of 86% [98]. The strong bisignated plasmonic CD signals were obtained, which could be reversed by altering the handiness of the nanoparticle arrangement along the helical path. Furthermore, the metafluid of Au nanoparticle assemblies with different handiness exhibited the opposite rotation direction of linearly polarized light, suggesting that the DNA origami structure could act as an effective tool for nanoparticle assemblies with desired optical or magnetic properties. DNA origami structures were also examined as a template to precisely organize anisotropic nanoparticles. Compared to 1D DNA bundles, 2D DNA origami has a larger dimension to accommodate anisotropic nanoparticles of big size. Wang *et al*. selected 2D origami structures with the DNA capture strand located at the opposite side as a template for synthesis of Au NR dimmers (Figure 1.10b). Six Au NR dimmers (X1, X2, L1, L2, T1, and T2) with different spatial configurations were achieved by changing the DNA capture strand at different sites [93]. All these Au nanorod dimmers exhibit distinct plasmonic CD response with bisignated shape, and the CD intensity decreased with transition of the Au dimmers gradually from X shape to T shape. Moreover, the plasmonic CD signals might be reversed by changing the configuration of the Au nanorod dimmers, demonstrating that the dipole–dipole interaction between Au nanorods was the dominating factor in the generation of plasmonic CD response.

Except for the static DNA structures, the dynamic DNA structures have been used for the construction of chiral plasmonic nanostructures. Ding

et al. deposited two linear Au nanospheres on a 2D rectangular DNA origami structure (Figure 1.11). Subsequently, the rectangular DNA origami structures were rolled up with the help of fuel DNA, resulting in fusion of two edges of the planar DNA origami into tube structure. As the Au nanoparticles were linearly placed on the plane DNA, the rolling up made them change to the helical 3D assembly. Accordingly, the plasmonic CD signal was arisen, and its intensity could be adjusted by changing the size of Au nanoparticles [99].

1.3.3.3 Inorganic-Channel-Induced Chiral Plasmonic Assembly

Thanks to fast development in syntheses of inorganic nanomaterials, many chiral structures such as chiral mesoporous silica (CMS) or helical ribbons have been widely prepared and studied [100–102]. In brief, by changing the experimental parameters such as pH value or mole ratio of reactants, molecules could form the chiral phase in the presence of silica precursors [103]. Afterward, the chiral template was removed from the cooperative assembly, giving rise to CMS. The detailed preparation of CMS can be found in a well-written review [23]. Owing to the presence of rich chirality inside the channel or on the surface, those chiral inorganic materials can be used as templates for the construction of chiral plasmonic nanostructures.

Che *et al*. synthesized CMS using chiral anionic surfactant *N*-acylamino acid and 3-aminopropyl-triethoxysilane as the costructure-directing agent (Figure 1.12). Three different types of chirality (the twist hexagonal morphology, the chiral arrangement of aminopropyl groups inside channel, and the helical channel orientation) were found to coexist in the CMS. In order to explore the different chiral effects on the plasmonic CD response, Ag nanoparticles were selectively *in situ* reduced onto the surface of CMS (Ag–CMS-as) into CMS with (Ag–CMS-ex) or without (Ag–CMS-cal) additional helical arrangement of amino groups. The CD spectroscopy measurement indicated that the optical activity of Ag–CMS-as was rather weak, while the CD signals of Ag–CMS-cal and Ag–CMS-ex were much stronger and had almost the same intensity. Thus, the authors deduced that the microscale helical surface was too large for Ag nanoparticles to induce strong optical activity, and the large CD intensity of Ag nanoparticle–CMS assembly was only obtained from the collectively asymmetric plasmonic interaction of Ag nanoparticles inside the channels [104].

The CMS system has been extended to films that respond to external environment changes. MacLachlan *et al*. synthesized free-standing CMS films by using chiral nanocrystalline cellulose (NCC) as a template [105]. After the removal of the chiral phase of NCC assembly from the silica film by calcinations of the film under air, free-standing CMS film was obtained. Owing to the existence of long-range helical structures in the films and the easily tuned optical property from UV to near IR region, CMS would be an ideal template for synthesis of chiral plasmonic structures. Chiral assembly of Ag nanoparticles in the template was observed to induce generation of plasmonic CD signal. After the CMS film loading with Ag nanoparticles was filled with water, change in the CD signal was obviously larger than that in the UV–vis spectrum, highlighting the potential application of optical activity from chiral nanostructures in sensors.

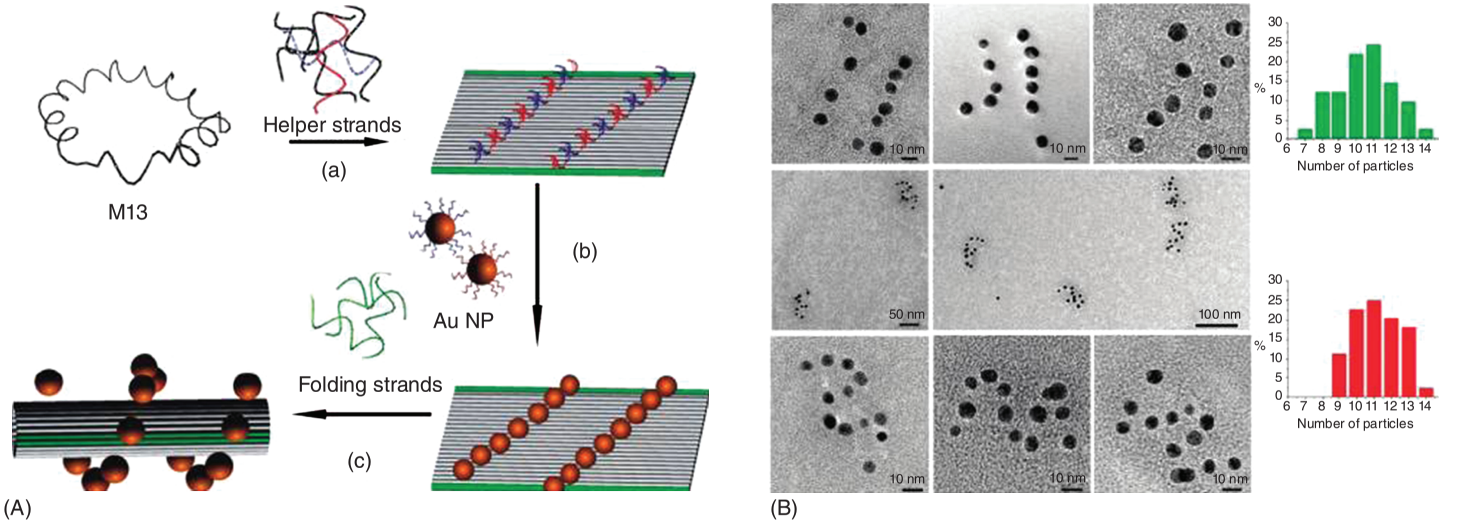

Figure 1.11 (A) Scheme and (B) TEM images of dynamic chiral assembly of nanoparticles. (Shen *et al*. 2011 [99]. Reproduced with permission of American Chemical Society.)

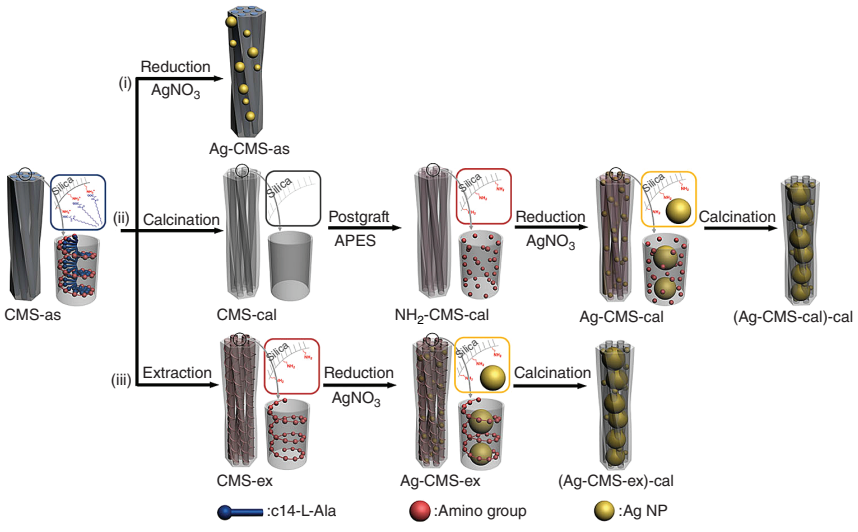

Figure 1.12 Chiral channel-induced Ag nanoparticle assembly. (Xie *et al*. 2012 [104]. Reproduced with permission of Wiley.)

Compared with soft templates, there are several limitations for hard templates to produce the chiral plasmonic nanostructures. First of all, since the size of the cavity is normally small, *in situ* reduction of metal ions is the only strategy for obtaining nanoparticles in the template. Therefore, the arrangement of metal nanoparticles by using the hard template is not controllable as those based on the soft template. Furthermore, the size of *in situ* synthesized metal nanoparticles is so small that the coupling among the metal nanoparticles is rather weak. In order to obtain strong optical activity, silver nanoparticles with strong plasmon resonance is often used for the chiral metal nanoparticles assembly on hard templates. The synthesis of large metal nanostructures in chiral mesoporous structures with strong CD response is still a big challenge Recently, Tang *et al*. adopted an alternative way in which Au nanorods were employed as the cores to be coated with the uniform CMS shells to fabricate the Au nanorod@CMS core–shell nanoparticles (Figure 1.13) [106]. These core–shell nanoparticles exhibited strong plasmonic

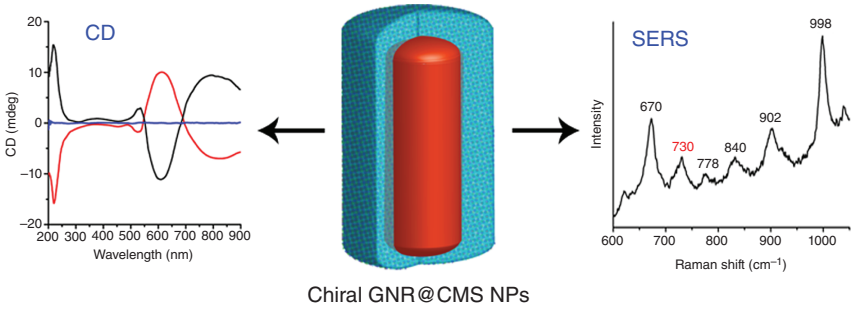

Figure 1.13 Au nanorod@CMS core–shell nanoparticles and its application in chiral recognition. (Liu *et al*. 2013 [106]. Reproduced with permission of American Chemical Society.)

CD signal in the visible and near-infrared region due to coupling between CMS shells and Au nanorod cores. Meanwhile, the CD signal could be fine-tuned by altering the aspect ratio of Au nanorods. Impressively, these Au nanorod@CMS core–shell nanoparticles displayed a great ability for highly special recognition of chiral molecules. These core–shell nanoparticles open another strategy for the construction of chiral metal nanoparticles with mesopores. It also can be image that complex chiral assembly of such core–shell nanoparticles could be obtained by tuning the particles' place, leading to a huge CD signal due to the strong plasmon intensity of nanoparticles.

1.4 Optical Application of Chiral Noble Metal Nanostructures

The unique optical activity of chiral noble metal nanostructures has been providing many new application opportunities. Compared with small organic or biological molecules that generally possess rather weak CD signal in UV light region, the chiral noble metal nanostructures of the sizes ranging from a few metal atoms to one hundred nanometers have been easily synthesized and its optical activity could be varied from the UV region to near-IR region. The strong CD responses of the chiral noble metal nanostructures might be achieved by increasing either the intrinsic chirality of small clusters or the coupling between metal nanoparticles and the chiral molecules. Furthermore, assembly of the noble metal nanoparticles into a chiral arrangement would greatly improve their CD responses. For example, Liz-Marzan *et al*. organized Au nanorods into the chiral nanostructure by using the chiral fibers as the template (Figure 1.14) and found that the anisotropic factor from the CD signal could be up to 0.022. Considering that the anisotropic factor of the molecules is normally below 0.005, it is reasonable to explore the chiral noble nanostructures of the strong and tunable optical activity as new optical materials and devices [80].

As many types of organic or biological molecules can be conjugated onto the chiral metal nanostructures and the resulting optical property is very sensitive to external environment change, chiral metal nanostructures are conveniently utilized in the field of sensors. The first type of sensors is based on the interaction between chiral molecule pairs. As an example, when L- or D-cysteine is modified onto the surface of Au nanoparticles, the pairwise zwitterionic dimerization is highly influenced by the surrounding nanoenvironment. Zhong *et al*. grafted chiral cysteine molecules onto Au nanoparticles for recognition of the enantiomers. The experimental result demonstrated that the assembly speed of Au nanoparticles modified with homochiral cysteine was at least 1 order magnitude faster than that of Au nanoparticles modified with heterochiral cysteine [107].

In addition to small molecule interactions, the immune-recognition effect or DNA specification interaction has been offering a wide platform for molecule detection. For instance, Kuang *et al*. firstly coated the bisphenol A antigen–oval albumin (BPA–OVA) or anti-BPA antibody onto the surface of Au nanoparticles of two different sizes through electrostatic attraction, respectively (Figure 1.15a).

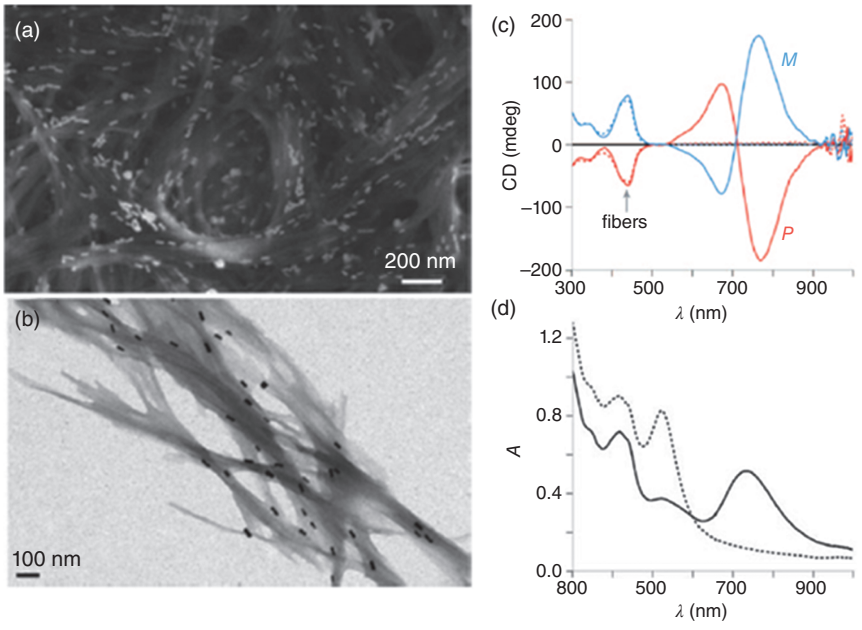

Figure 1.14 (a) Typical SEM and (b) TEM images (a, b) of chiral Au nanorod assembly and its corresponding (c) CD signal and (d) UV–vis spectrum. (Guerrero-Martinez *et al*. 2011 [80]. Reproduced with permission of Wiley.)

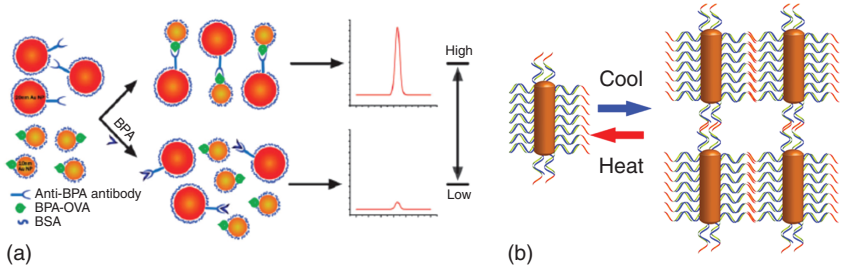

Figure 1.15 Scheme of detection strategy based on (a) immune-recognition. (Xu *et al*. 2012 [108]. Reproduced with permission of Royal Society of Chemistry.) and (b) DNA detection. (Li *et al*. 2012 [109]. Reproduced with permission of American Chemical Society.)

Afterward, the anti-BPA antibody was used to connect two Au nanoparticles to form the asymmetric dimmers upon the biorecognition between antibody and antigen, giving rise to considerable enhancement of the plasmonic CD intensity. Finally, the target BPA molecules were introduced, and the competition recognition of anti-BPA antibodies to the BPA molecules and the BPA–OVA antigen made Au nanoparticles being as the dispersed state instead of the aggregation, leading to decrease in the plasmonic CD intensity. The linear range of detection cover three orders of magnitudes and the LOD is as low as 0.02 ppb [108].

Tang *et al*. took advantage of the reversible plasmonic CD signals for DNA detection (Figure 1.15b) [109]. In the Au nanorod and DNA assembly, the coupling between chiral signal of DNA and SPR characteristic of Au nanorods resulted in generation of the plasmonic CD response the visible light region. By reducing the temperature below the melting temperature of the sticky end of DNA chains, Au nanorod assembly happened as the sticky end connected with each other, leading to an obvious enhancement in the plasmonic CD intensity and a great change of the lineshape of CD signal. As compassion, the contrast DNA without stick end could not cause Au nanorod assembly and the corresponding plasmonic CD would not increase. Thus, the change in the plasmonic CD intensity was a good candidate for high sensitive detection of DNA molecules, and our experimental results proved that the detection limit based on the plasmonic CD response was comparable to or even lower than that with the conventional colorimetric detection methods. What was more, the temperature-dependent CD signal was very stable in different temperature change cycles, providing a reliable way to avoid bias of signal detection. Recently, Kotov *et al*. further demonstrated that the detect limit of DNA molecules could be as low as 3.7 aM upon change in the plasmonic CD of chiral Au nanorod assembly. It is worth mentioning that the detection limit based on side-by-side assembly of Au nanorods was much lower than that obtained with other optical detection methods such as UV–vis absorption, fluorescence, or surface-enhanced Raman scattering (SERS) [110].

Because many DNA structures have the special interactions with some target molecules, the DNA modified chiral metal nanostructures should be a versatile platform for detection of different species [111]. Xu *et al*. measured the concentration of Hg^{2+} ions in solution by using the plasmonic CD signal of DNA-modified Au nanorods, Au nanorod assembly was formed with addition of Hg^{2+} ions, which was reasonable because Hg^{2+} ions induced formation of T-Hg^{2+}-T base pair in the DNA sequences that were grafted onto the surface of Au nanorods. The strong coupling between Au nanorods in the assembly gave rise to the formation of the obviously enhanced CD intensity. The linear relationship between the plasmonic CD intensity and the concentration of Hg^{2+} ions was in a broad range of 0.05–10 ng/ml [112].

1.5 Perspectives

In the past few years, chiral noble metal nanostructures including the clusters, plasmonic nanoparticles, and plasmonic assembly have been widely reported, providing a new route for the construction of the artificial materials with novel property and functionality. It should be stressed that though the remarkable progresses have achieved, the field of chiral noble metal nanostructures is still at the burgeon stage and many great challenges are waiting for be overcome.

First of all, we need to develop and improve the theory about the origin and optical activity of chiral nanostructures. Current understanding of the origin of the chiral nanostructures could be classified into three mechanisms: (i) intrinsic chirality of nanoparticles, (ii) coupling between chiral molecules and metal

nanoparticles, and (iii) the chiral arrangement of nanoparticles. Unfortunately, these mechanisms normally happened simultaneously, especially when there are chiral molecules present in the system, which make elucidation of chirality origin become difficult. Moreover, although many theories have been proposed for understanding of optical activity of the chiral nanostructures, most of them are based on dipole–dipole interactions and the complex of nanoparticles shape and morphology are not taken into account. For example, Gang *et al*. found that the Ag nanocubes with 42-nm edge length enhanced CD signal of the ssDNA about 100 times, while other nanoparticles such as Au nanocubes, nanospheres, and nanooctahedron showed no evidence of CD enhancement [113]. Such an abnormal phenomenon calls for a deep understanding of the origin of the CD response. On the other side, the experiment verification of theory should accompany the development of theory. As an example, accurate control of the arrangement of plasmonic nanoparticles in the assembly would provide a direct link between the experimental measurement and the theoretical analysis.

Second, although chiral noble metal structures with rather strong CD signals have been obtained in the past few years, construction of different chiral metal nanostructures, especially with response to external stimuli and extremely high optical activity, still remains highly difficult. In order to fabricate such chiral noble metal nanostructures, special attention should be paid to the chiral cores of the noble metal clusters, the coupling efficiency between SPR characteristics of noble metal nanoparticles and chiral molecules, and asymmetric framework design of chiral nanoparticle assembly. Furthermore, in order to application of chiral metal nanostructure as the smart materials, the responses to different external stimuli should be considered prior to construction of chiral noble metal nanostructures.

Last but not least, current applications about the optical activity of chiral metal nanoparticles are mostly focused on sensors or biosensors. To extend the application potential of the optical activity at nanoscale size becomes one of key issues in the future study. For example, since the chiral noble metal nanostructures exhibit strong and reproducible plasmonic CD response in the visible light region, it is reasonable to ask whether we can develop a new type of microscopy, CD microscopy, for bioimaging and biodiagnosis. The advantages of plasmonic nanostructures based on CD microscopy are significant: The strong and near field plasmonic response at the visible light region can effectively exclude possible influence of most biological molecules that usually possess the CD signal at the UV light region. Furthermore, the plasmonic CD response is sensitive to the spatial arrangement, which will provide a unique insight into the biological process, for example, folding or unfolding of peptide, or DNA in cells or organs.

In summary, chiral noble metal nanostructures have been one of the hottest research topics in the field of nanoscience in the last several years. Until now, scientists only touch the tip of the iceberg, and we are optimistic that many important findings about the chiral noble metal nanostructures will be made in the near future.

References

1 Bradshaw, D., Claridge, J.B., Cussen, E.J., Prior, T.J., and Rosseinsky, M.J. (2005) *Acc. Chem. Res.*, **38**, 273–282.
2 Palmans, A.R.A. and Meijer, E.W. (2007) *Angew. Chem. Int. Ed.*, **46**, 8948–8968.
3 Feringa, B.L., van Delden, R.A., Koumura, N., and Geertsema, E.M. (2000) *Chem. Rev.*, **100**, 1789–1816.
4 Green, M.M. and Jain, V. (2010) *Origins Life Evol. B*, **40**, 111–118.
5 Smith, D.R. and Kroll, N. (2000) *Phys. Rev. Lett.*, **85**, 2933–2936.
6 Soukoulis, C.M., Kafesaki, M., and Economou, E.N. (2006) *Adv. Mater.*, **18**, 1941–1952.
7 Seo, J.S., Whang, D., Lee, H., Jun, S.I., Oh, J., Jeon, Y.J., and Kim, K. (2000) *Nature*, **404**, 982–986.
8 Trost, B.M. and VanVranken, D.L. (1996) *Chem. Rev.*, **96**, 395–422.
9 Trost, B.M. and Brindle, C.S. (2010) *Chem. Soc. Rev.*, **39**, 1600–1632.
10 Zhu, G.D. and Okamura, W.H. (1995) *Chem. Rev.*, **95**, 1877–1952.
11 Wang, Y., Xu, J., Wang, Y., and Chen, H. (2013) *Chem. Soc. Rev.*, **42**, 2930–2962.
12 Ben-Moshe, A., Maoz, B.M., Govorov, A.O., and Markovich, G. (2013) *Chem. Soc. Rev.*, **42**, 7028–7041.
13 Halas, N.J., Lal, S., Chang, W.S., Link, S., and Nordlander, P. (2011) *Chem. Rev.*, **111**, 3913–3961.
14 Niu, W., Zheng, S., Wang, D., Liu, X., Li, H., Han, S., Chen, J., Tang, Z., and Xu, G. (2008) *J. Am. Chem. Soc.*, **131**, 697–703.
15 Xia, Y., Xiong, Y., Lim, B., and Skrabalak, S.E. (2009) *Angew. Chem. Int. Ed.*, **48**, 60–103.
16 Zhou, Y.L., Zhu, Z.N., Huang, W.X., Liu, W.J., Wu, S.J., Liu, X.F., Gao, Y., Zhang, W., and Tang, Z.Y. (2011) *Angew. Chem. Int. Ed.*, **50**, 11456–11459.
17 Jin, R.C., Cao, Y.W., Mirkin, C.A., Kelly, K.L., Schatz, G.C., and Zheng, J.G. (2001) *Science*, **294**, 1901–1903.
18 Fan, Z.Y., Zhang, H., and Govorov, A.O. (2013) *J. Phys. Chem. C*, **117**, 14770–14777.
19 Albanese, A., Tang, P.S., and Chan, W.C.W. (2012) *Annu. Rev. Biomed. Eng.*, **14**, 1–16.
20 Jiang, W., Kim, B.Y.S., Rutka, J.T., and Chan warren, C.W. (2008) *Nat. Nanotechnol.*, **3**, 145–150.
21 Li, Y., Zhou, Y., Wang, H.-Y., Perrett, S., Zhao, Y., Tang, Z., and Nie, G. (2011) *Angew. Chem. Int. Ed.*, **50**, 5860–5864.
22 Noguez, C. and Garzon, I.L. (2009) *Chem. Soc. Rev.*, **38**, 757–771.
23 Qiu, H. and Che, S. (2011) *Chem. Soc. Rev.*, **40**, 1259–1268.
24 Aggeli, A., Nyrkova, I.A., Bell, M., Harding, R., Carrick, L., McLeish, T.C.B., Semenov, A.N., and Boden, N. (2001) *Proc. Natl. Acad. Sci. U. S. A.*, **98**, 11857–11862.
25 Crassous, J. (2009) *Chem. Soc. Rev.*, **38**, 830–845.
26 Hannah, K.C. and Armitage, B.A. (2004) *Acc. Chem. Res.*, **37**, 845–853.

27 Warnke, I. and Furche, F. (2012) *Wiley Interdiscip. Rev.: Comput. Mol. Sci.*, **2**, 150–166.
28 Berova, N., Nakanishi, K., and Woody, R.W. (2000) *Circular Dichroism: Principles and Applications*, 2nd edn, New York, Wiley-VCH.
29 Bringmann, G., Messer, K., Wohlfarth, M., Kraus, J., Dumbuya, K., and Rückert, M. (1999) *Anal. Chem.*, **71**, 2678–2686.
30 Miles, A.J. and Wallace, B.A. (2006) *Chem. Soc. Rev.*, **35**, 39–51.
31 Qian, H., Zhu, M., Wu, Z., and Jin, R. (2012) *Acc. Chem. Res.*, **45**, 1470–1479.
32 Tamura, M. and Fujihara, H. (2003) *J. Am. Chem. Soc.*, **125**, 15742–15743.
33 Negishi, Y., Nobusada, K., and Tsukuda, T. (2005) *J. Am. Chem. Soc.*, **127**, 5261–5270.
34 Garzón, I.L., Reyes-Nava, J.A., Rodríguez-Hernández, J.I., Sigal, I., Beltrán, M.R., and Michaelian, K. (2002) *Phys. Rev. B*, **66**, 073403.
35 Goldsmith, M.R., George, C.B., Zuber, G., Naaman, R., Waldeck, D.H., Wipf, P., and Beratan, D.N. (2006) *Phys. Chem. Chem. Phys.*, **8**, 63–67.
36 Gautier, C. and Bürgi, T. (2006) *J. Am. Chem. Soc.*, **128**, 11079–11087.
37 Sánchez-Castillo, A., Noguez, C., and Garzón, I.L. (2010) *J. Am. Chem. Soc.*, **132**, 1504–1505.
38 Jadzinsky, P.D., Calero, G., Ackerson, C.J., Bushnell, D.A., and Kornberg, R.D. (2007) *Science*, **318**, 430–433.
39 Zeng, C., Li, T., Das, A., Rosi, N.L., and Jin, R. (2013) *J. Am. Chem. Soc.*, **135**, 10011–10013.
40 Lopez-Acevedo, O., Tsunoyama, H., Tsukuda, T., Häkkinen, H., and Aikens, C.M. (2010) *J. Am. Chem. Soc.*, **132**, 8210–8218.
41 Qian, H., Eckenhoff, W.T., Zhu, Y., Pintauer, T., and Jin, R. (2010) *J. Am. Chem. Soc.*, **132**, 8280–8281.
42 Lopez-Acevedo, O., Akola, J., Whetten, R.L., Grönbeck, H., and Häkkinen, H. (2009) *J. Phys. Chem. C*, **113**, 5035–5038.
43 Schaaff, T.G., Knight, G., Shafigullin, M.N., Borkman, R.F., and Whetten, R.L. (1998) *J. Phys. Chem. B*, **102**, 10643–10646.
44 Schaaff, T.G. and Whetten, R.L. (2000) *J. Phys. Chem. B*, **104**, 2630–2641.
45 Yao, H., Miki, K., Nishida, N., Sasaki, A., and Kimura, K. (2005) *J. Am. Chem. Soc.*, **127**, 15536–15543.
46 Yao, H., Fukui, T., and Kimura, K. (2007) *J. Phys. Chem. C*, **111**, 14968–14976.
47 Nishida, N., Yao, H., Ueda, T., Sasaki, A., and Kimura, K. (2007) *Chem. Mater.*, **19**, 2831–2841.
48 Nishida, N., Yao, H., and Kimura, K. (2008) *Langmuir*, **24**, 2759–2766.
49 Si, S., Gautier, C., Boudon, J., Taras, R., Gladiali, S., and Bürgi, T. (2009) *J. Phys. Chem. C*, **113**, 12966–12969.
50 Knoppe, S., Dharmaratne, A.C., Schreiner, E., Dass, A., and Bürgi, T. (2010) *J. Am. Chem. Soc.*, **132**, 16783–16789.
51 Dolamic, I., Knoppe, S., Dass, A., and Bürgi, T. (2012) *Nat. Commun.*, **3**, 798.
52 Knoppe, S., Dolamic, I., and Bürgi, T. (2012) *J. Am. Chem. Soc.*, **134**, 13114–13120.

53 Knoppe, S., Dolamic, I., Dass, A., and Bürgi, T. (2012) *Angew. Chem. Int. Ed.*, **51**, 7589–7591.

54 Gao, Y. and Tang, Z. (2011) *Small*, **7**, 2133–2146.

55 Wang, X.S., Zou, Y.C., Zhu, J.R., and Wang, Y. (2013) *J. Phys. Chem. C*, **117**, 14197–14205.

56 Ben-Moshe, A., Maoz, B., Govorov, A.O., and Markovich, G. (2013) *Chem. Soc. Rev.*, **42**, 7028–7041.

57 Gong, J., Li, G., and Tang, Z. (2012) *Nano Today*, **7**, 564–585.

58 Bishop, K.J.M., Wilmer, C.E., Soh, S., and Grzybowski, B.A. (2009) *Small*, **5**, 1600–1630.

59 Valev, V.K., Baumberg, J.J., Sibilia, C., and Verbiest, T. (2013) *Adv. Mater.*, **25**, 2517–2534.

60 Fan, Z.Y. and Govorov, A.O. (2012) *Nano Lett.*, **12**, 3283–3289.

61 Yeom, B., Zhang, H., Zhang, H., Park, J.I., Kim, K., Govorov, A.O., and Kotov, N.A. (2013) *Nano Lett.*, **13**, 5277–5283.

62 Govorov, A.O. (2011) *J. Phys. Chem. C*, **115**, 7914–7923.

63 Govorov, A.O., Fan, Z., Hernandez, P., Slocik, J.M., and Naik, R.R. (2010) *Nano Lett.*, **10**, 1374–1382.

64 Govorov, A.O. and Fan, Z. (2012) *ChemPhysChem*, **13**, 2551–2560.

65 Itai, L., Gabriel, S., Tcipi, F., Edward, K., and Gil, M. (2008) *Angew. Chem. Int. Ed.*, **47**, 4855–4857.

66 Abdulrahman, N.A., Fan, Z., Tonooka, T., Kelly, S.M., Gadegaard, N., Hendry, E., Govorov, A.O., and Kadodwala, M. (2012) *Nano Lett.*, **12**, 977–983.

67 Fan, Z. and Govorov, A.O. (2010) *Nano Lett.*, **10**, 2580–2587.

68 Fan, Z. and Govorov, A.O. (2011) *J. Phys. Chem. C*, **115**, 13254–13261.

69 Auguie, B., Alonso-Gomez, J.L., Guerrero-Martinez, A., and Liz-Marzan, L.M. (2011) *J. Phys. Chem. Lett.*, **2**, 846–851.

70 Yan, W., Ma, W., Kuang, H., Liu, L., Wang, L., Xu, L., and Xu, C. (2013) *J. Phys. Chem. C*, **117**, 17757–17765.

71 Maoz, B.M., van der Weegen, R., Fan, Z., Govorov, A.O., Ellestad, G., Berova, N., Meijer, E.W., and Markovich, G. (2012) *J. Am. Chem. Soc.*, **134**, 17807–17813.

72 Shemer, G., Krichevski, O., Markovich, G., Molotsky, T., Lubitz, I., and Kotlyar, A.B. (2006) *J. Am. Chem. Soc.*, **128**, 11006–11007.

73 Tamarin, T., Moshe, A.B., Markovich, G., and Kotlyar, A.B. (2010) *J. Phys. Chem. C*, **114**, 15951–15954.

74 Slocik, J.M., Govorov, A.O., and Naik, R.R. (2011) *Nano Lett.*, **11**, 701–705.

75 Layani, M.E., Ben Moshe, A., Varenik, M., Regev, O., Zhang, H., Govorov, A.O., and Markovich, G. (2013) *J. Phys. Chem. C*, **117**, 22240–22244.

76 Zhu, Z., Liu, W., Li, Z., Han, B., Zhou, Y., Gao, Y., and Tang, Z. (2012) *ACS Nano*, **6**, 2326–2332.

77 Zhu, Z., Guo, J., Liu, W., Li, Z., Han, B., Zhang, W., and Tang, Z. (2013) *Angew. Chem. Int. Ed.*, **52**, 13571–13575.

78 Leroux, F., Gysemans, M., Bals, S., Batenburg, K.J., Snauwaert, J., Verbiest, T., Van Haesendonck, C., and Van Tendeloo, G. (2010) *Adv. Mater.*, **22**, 2193–2197.

79 Zhu, L., Li, X., Wu, S., Nguyen, K.T., Yan, H., Ågren, H., and Zhao, Y. (2013) *J. Am. Chem. Soc.*, **135**, 9174–9180.
80 Guerrero-Martinez, A., Auguie, B., Alonso-Gomez, J.L., Dzolic, Z., Gomez-Grana, S., Zinic, M., Cid, M.M., and Liz-Marzan, L.M. (2011) *Angew. Chem. Int. Ed.*, **50**, 5499–5503.
81 Oh, H.S., Liu, S., Jee, H., Baev, A., Swihart, M.T., and Prasad, P.N. (2010) *J. Am. Chem. Soc.*, **132**, 17346–17348.
82 Aili, D., Enander, K., Rydberg, J., Nesterenko, I., Björefors, F., Baltzer, L., and Liedberg, B. (2008) *J. Am. Chem. Soc.*, **130**, 5780–5788.
83 Ulijn, R.V. and Smith, A.M. (2008) *Chem. Soc. Rev.*, **37**, 664–675.
84 Song, C., Blaber, M.G., Zhao, G., Zhang, P., Fry, H.C., Schatz, G.C., and Rosi, N.L. (2013) *Nano Lett.*, **13**, 3256–3261.
85 George, J. and Thomas, K.G. (2010) *J. Am. Chem. Soc.*, **132**, 2502–2503.
86 Han, D., Pal, S., Nangreave, J., Deng, Z., Liu, Y., and Yan, H. (2011) *Science*, **332**, 342–346.
87 Jones, M.R., Macfarlane, R.J., Lee, B., Zhang, J., Young, K.L., Senesi, A.J., and Mirkin, C.A. (2010) *Nat. Mater.*, **9**, 913–917.
88 Seeman, N. (2007) *Mol. Biotechnol.*, **37**, 246–257.
89 Park, S.Y., Lytton-Jean, A.K.R., Lee, B., Weigand, S., Schatz, G.C., and Mirkin, C.A. (2008) *Nature*, **451**, 553–556.
90 Mastroianni, A.J., Claridge, S.A., and Alivisatos, A.P. (2009) *J. Am. Chem. Soc.*, **131**, 8455–8459.
91 Chen, W., Bian, A., Agarwal, A., Liu, L., Shen, H., Wang, L., Xu, C., and Kotov, N.A. (2009) *Nano Lett.*, **9**, 2153–2159.
92 Yan, W., Xu, L., Xu, C., Ma, W., Kuang, H., Wang, L., and Kotov, N.A. (2012) *J. Am. Chem. Soc.*, **134**, 15114–15121.
93 Lan, X., Chen, Z., Dai, G., Lu, X., Ni, W., and Wang, Q. (2013) *J. Am. Chem. Soc.*, **135**, 11441–11444.
94 Rothemund, P.W.K. (2006) *Nature*, **440**, 297–302.
95 Douglas, S.M., Dietz, H., Liedl, T., Hoegberg, B., Graf, F., and Shih, W.M. (2009) *Nature*, **459**, 414–418.
96 Ke, Y., Douglas, S.M., Liu, M., Sharma, J., Cheng, A., Leung, A., Liu, Y., Shih, W.M., and Yan, H. (2009) *J. Am. Chem. Soc.*, **131**, 15903–15908.
97 Sacca, B. and Niemeyer, C.M. (2012) *Angew. Chem. Int. Ed.*, **51**, 58–66.
98 Kuzyk, A., Schreiber, R., Fan, Z., Pardatscher, G., Roller, E.-M., Hogele, A., Simmel, F.C., Govorov, A.O., and Liedl, T. (2012) *Nature*, **483**, 311–314.
99 Shen, X., Song, C., Wang, J., Shi, D., Wang, Z., Liu, N., and Ding, B. (2011) *J. Am. Chem. Soc.*, **134**, 146–149.
100 Li, Y., Li, B., Yan, Z., Xiao, Z., Huang, Z., Hu, K., Wang, S., and Yang, Y. (2013) *Chem. Mater.*, **25**, 307–312.
101 Che, S., Liu, Z., Ohsuna, T., Sakamoto, K., Terasaki, O., and Tatsumi, T. (2004) *Nature*, **429**, 281–284.
102 Shopsowitz, K.E., Qi, H., Hamad, W.Y., and MacLachlan, M.J. (2010) *Nature*, **468**, 422–425.
103 Jin, H., Liu, Z., Ohsuna, T., Terasaki, O., Inoue, Y., Sakamoto, K., Nakanishi, T., Ariga, K., and Che, S. (2006) *Adv. Mater.*, **18**, 593–596.
104 Xie, J., Duan, Y., and Che, S. (2012) *Adv. Funct. Mater.*, **22**, 3784–3792.

105 Qi, H., Shopsowitz, K.E., Hamad, W.Y., and MacLachlan, M.J. (2011) *J. Am. Chem. Soc.*, **133**, 3728–3731.
106 Liu, W., Zhu, Z., Deng, K., Li, Z., Zhou, Y., Qiu, H., Gao, Y., Che, S., and Tang, Z. (2013) *J. Am. Chem. Soc.*, **135**, 9659–9664.
107 Lim, I.I.S., Mott, D., Engelhard, M.H., Pan, Y., Kamodia, S., Luo, J., Njoki, P.N., Zhou, S., Wang, L., and Zhong, C.J. (2008) *Anal. Chem.*, **81**, 689–698.
108 Xu, Z., Xu, L., Zhu, Y., Ma, W., Kuang, H., Wang, L., and Xu, C. (2012) *Chem. Commun.*, **48**, 5760–5762.
109 Li, Z., Zhu, Z., Liu, W., Zhou, Y., Han, B., Gao, Y., and Tang, Z. (2012) *J. Am. Chem. Soc.*, **134**, 3322–3325.
110 Ma, W., Kuang, H., Xu, L., Ding, L., Xu, C., Wang, L., and Kotov, N.A. (2013) *Nat. Commun.*, **4**, 2689.
111 Wu, X., Xu, L., Liu, L., Ma, W., Yin, H., Kuang, H., Wang, L., Xu, C., and Kotov, N.A. (2013) *J. Am. Chem. Soc.*, **135**, 18629–18636.
112 Zhu, Y., Xu, L., Ma, W., Xu, Z., Kuang, H., Wang, L., and Xu, C. (2012) *Chem. Commun.*, **48**, 11889–11891.
113 Lu, F., Tian, Y., Liu, M., Su, D., Zhang, H., Govorov, A.O., and Gang, O. (2013) *Nano Lett.*, **13**, 3145–3151.